sustainability

MDPI

Article

CFD-Guided Evaluation of Spark-Assisted Gasoline Compression Ignition for Cold Idle Operation

Le Zhao [1,*], Yu Zhang [1], Yuanjiang Pei [1], Anqi Zhang [1] and Muhsin M Ameen [2]

[1] Aramco Americas: Aramco Research Center—Detroit, Novi, MI 48377, USA; yu.zhang@aramcoamericas.com (Y.Z.); Yuanjiang.Pei@aramcoamericas.com (Y.P.); Anqi.Zhang@aramcoamericas.com (A.Z.)
[2] Argonne National Laboratory, Lemont, IL 60439, USA; mameen@anl.gov
* Correspondence: le.zhao@aramcoamericas.com

Abstract: A closed-cycle, three-dimensional (3D) computational fluid dynamics (CFD) analysis campaign was conducted to evaluate the performance of using spark plugs to assist gasoline compression ignition (GCI) combustion during cold idle operations. A conventional spark plug using single-sided J-strap design was put at a location on the cylinder head to facilitate spray-guided spark assistance. Ignition was modeled with an L-type energy distribution to depict the breakdown and the arc-to-glow phases during the energy discharge process. Several key design parameters were investigated, including injector clocking, number of nozzle holes, spray inclusion angle, number of fuel injections, fuel split ratio, and fuel injection timings. The study emphasized the region around the spark gap, focusing on flame kernel formation and development and local equivalence ratio distribution. Flame kernel development and the ignition process were found to correlate strongly with the fuel stratification and the flow velocity near the spark gap. The analysis results showed that the flame kernel development followed the direction of the local flow field. In addition, the local fuel stratification notably influenced early-stage flame kernel development due to varying injection spray patterns and the fuel injection strategies. Among these design parameters, the number of nozzle holes and fuel injection timing had the most significant effects on the engine combustion performance.

Keywords: CFD; spark-assisted; cold start; gasoline compression ignition

Citation: Zhao, L.; Zhang, Y.; Pei, Y.; Zhang, A.; Ameen, M.M. CFD-Guided Evaluation of Spark-Assisted Gasoline Compression Ignition for Cold Idle Operation. *Sustainability* **2021**, *13*, 13096. https://doi.org/10.3390/su132313096

Academic Editors: Luca Marchitto and Cinzia Tornatore

Received: 11 October 2021
Accepted: 23 November 2021
Published: 26 November 2021

1. Introduction

Regulatory demand for reducing vehicle criteria pollutants and CO_2 emissions is increasing around the world. As a result, several advanced engine combustion strategies that have the potential to achieve clean high-efficiency combustion have been proposed and extensively studied [1–9]. Gasoline compression ignition (GCI) [10–15] is one of the most well-known low temperature combustion strategies. GCI has gained attention in recent years because of its potential to harness gasoline's low reactivity to enhance partially premixed compression ignition, whereby high fuel efficiency is achieved while engine-out NO_x and soot emissions are reduced.

However, GCI combustion can be challenging under cold conditions. The implications of gasoline's high volatility and low reactivity on spray evaporation, fuel-air mixing, and ignition under very cold conditions have not been clearly established [16–19]. It is essential to develop a combustion strategy that allows robust and clean GCI combustion during cold operation. In our previous work, we investigated the ignitability of different gasoline fuels and evaluated the influence of pressure and temperature on gasoline autoignition at different equivalence ratios numerically, without considering any forced ignition assistance [17]. We observed a trend toward lower ignitability as lower reactivity (i.e., lower cetane) fuels were used. We also generated thermodynamic maps of ignitability for the fuels at a wide range of operating conditions from cold idle to full warm-up.

In addition, during cold start operation, forced ignition assistances such as glow plugs have been commonly used in diesel engines to increase the local temperature and promote vaporization prior to the mixture preparation process [20]. Our previous studies employed 3D combustion CFD analysis to investigate the effect of a glow plug assistance on gasoline autoignition and the subsequent combustion process at cold idle in a heavy-duty GCI engine [21]. We found that combustion efficiency was improved and CA50 was advanced by increasing the glow plug surface temperature. Moreover, the interaction between the glow plug and the spray plumes had an effect on promoting combustion. In addition to glow plug assistance, we also studied spark-assisted cold idle operation by investigating the influence of spark plug orientation and spark timing on the ignition and combustion processes [22]. We found that complex flow-geometry interactions in the confined spark gap volume dictated the early flame kernel development. Specifically, the interaction between the spray plume and the spark plug electrode could be sensitive to the spark plug orientation and the spark timing.

Building on previous spark-assistance work, we conducted a thorough evaluation of the injector spray pattern and the fuel injection strategy to gain insight into their impacts on flame kernel development, equivalence ratio distribution near the spark gap, and global combustion characteristics. Particular emphasis was placed on studying the effects of several key design variables, including injector clocking, number of nozzle holes, spray inclusion angle, fuel split ratio, and fuel injection timings.

2. Methodology

2.1. Experimental Setup

Combustion simulations were based on the experimental data generated from a 2013 model year Cummins ISX15 on-highway, heavy-duty diesel engine [17,19]. The key engine specifications and baseline cold idle operating conditions are listed in Table 1. Note that the cold idle conditions in this work are in point of fact the cold federal test procedure (FTP) idle at normal ambient temperature.

Table 1. Experimental engine specifications and baseline operating conditions during cold idle.

Engine Specifications	
Stroke (mm)	169
Bore (mm)	137
Connecting rod length (mm)	262
Displacement volume (L)	14.9
Number of cylinders	6
Compression ratio	17.3:1
Diesel fuel system	2500 bar common rail
Operating Conditions	
Speed (r/min.)	600
Swirl ratio	1
NMEP (kPa)	~100
EGR rate (-)	0
Intake valve closing (°ATDC)	−137
Exhaust valve opening (°ATDC)	148
Intake manifold pressure (kPa)	113
Intake manifold temperature (°C)	26
Oil gallery temperature (°C)	50
Coolant temperature (°C)	27
Injection pressure (bar)	300
Injection strategy	Split
Fueling (mg/cycle/cylinder)	27.6
Split ratio	4:6
SOI_{1st}/SOI_{2nd} (°ATDC)	−30/−16

2.2. CFD Model Description

The commercial software CONVERGE v2.4 [23] was utilized to carry out the closed-cycle 3D CFD simulations from intake valve closing (IVC) to exhaust valve opening (EVO). A 360° mesh representing one full cylinder was employed in the simulations. As shown in Figure 1, a conventional spark plug, with single-sided J-strap design, was placed on the cylinder head and close to the centrally mounted injector to study the performance of a spray-guided spark-assistance strategy. The distance between the spark plug and the injector was about 15 mm; the protruding length from cylinder head to the center of spark gap was approximately 3.6 mm. Ignition was modeled with an L-type energy distribution and the details on energy distribution during the breakdown and the arc/glow phases can be found in our previous work [22].

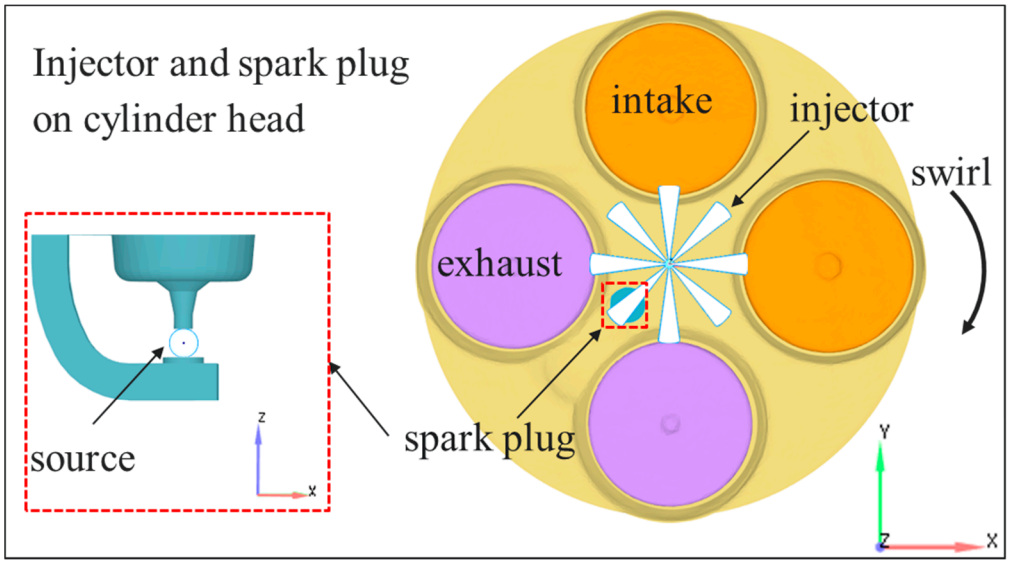

Figure 1. Injector and spark plug location through cylinder head.

A Reynolds-averaged Navier–Stokes (RANS)-based renormalization group (RNG) k-ε turbulence model was used to simulate the in-cylinder flow, while the combustion was modeled via a detailed chemistry solver that treats each computational cell being as a well-stirred reactor. The autoignition, and the subsequent combustion process, was simulated using the reduced primary reference fuel (PRF) mechanism from Liu et al. [24], which contained 44 species and 139 reactions. This reduced PRF mechanism showed good agreement against experiments when simulating the combustion of a GCI engine [19,25]. NO_x emissions were predicted by a reduced mechanism including 4 species and 13 reactions [26,27]. It is worth noting that the simplification on the closure of turbulent-chemistry interaction by the present combustion model may lead to discrepancies, particularly under the reduced reactive cold operations [28]. Moreover, spray models based on the Lagrangian discrete droplet approach were used to simulate the fuel injection process; these spray sub-models have been extensively validated at wide-ranging operations in previous studies [29–31]. Table 2 lists the primary CONVERGE sub-models used in current study.

The base mesh size for our simulations was 1.4 mm. Adaptive Mesh Refinement (AMR) activated on velocity and temperature gradients was used to refine the mesh to 0.35 mm across the computational domain. Fixed embedding refinement with a level of 1 was added permanently to accurately predict the flow near the wall, while a level of 2 was enforced on the injector to better capture the spray dynamics. Furthermore, two spherical embedding levels of 2 and 3 were across the spark gap during spark event to reduce the mesh size to allow for accurate prediction of the flame kernel development.

Table 2. CFD details.

Spray, Combustion, and Emission Models	
Injection	Blob
Drag-law	Dynamic
Evaporation	Frossling
Collision	NTC
Break-up	Modified KH-RT
Combustion solver	Well-stirred reactor
Fuel surrogate	PRF92
Chemical kinetic mechanism	Liu et al. [24]
NO_x	4 species and 13 reactions [26,27]
Turbulence	RNG k-ε
Wall heat transfer	O'Rourke and Amsden
Mesh Size	
Base	1.4 mm
AMR level	2 on velocity and temperature gradients
Fixed embedding level	1 in head and piston, 2 in injector, 2 and 3 in spark gap

A mesh refinement study with three different minimum mesh sizes (0.35 mm, 0.175 mm, and 0.0875 mm) surrounding the spark plug was performed. Simulations with minimum mesh sizes were performed using two to four levels of refinement near the spark plug-embedded region. For the sake of brevity, Figure 2 depicts only the in-cylinder pressure and apparent heat release rate (AHRR) results obtained for the different mesh resolutions. Finally, considering the mesh convergence and computational demands, the 0.175 mm mesh size was selected as the reference minimum mesh size for the remainder of the study. Note that CFD model validation against engine experimental results during cold idle has been performed in Zhao et al. [17,21].

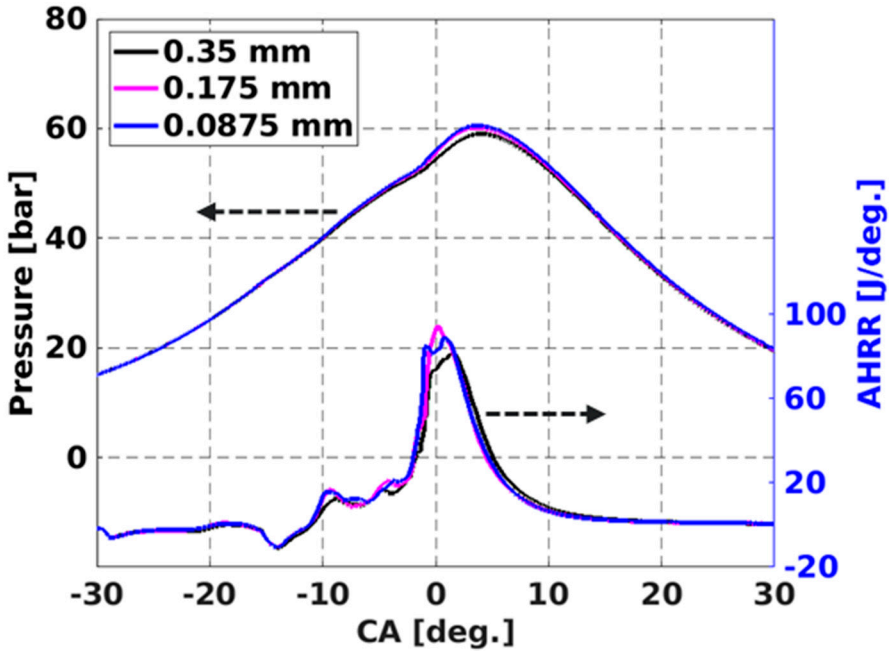

Figure 2. In-cylinder pressure and apparent heat release rate (AHRR) for different mesh size cases (black: 0.35 mm, magenta: 0.175 mm, blue: 0.0875 mm).

3. Results and Discussions

3.1. Design Variables

Several design variables on the injector spray pattern and fuel injection strategy were evaluated in this work, including injector clocking, number of nozzle holes, spray inclusion angle, fuel split ratio, injection timings, and Δ_1 representing the difference between the spark timing and the first start of injection timing (SOI_{1st}). The investigative range for these design variables is summarized in Table 3. These parameters were studied one at a time.

Table 3. Design parameters and investigation range.

Parameters	Range	Baseline
Injector clocking (°)	−20 to 20	0
Number of nozzle holes	7 to 14	8
Spray inclusion angle φ (°)	140 to 156	148
Fuel split ratio	2:8 to 10:0 (single injection)	4:6
SOI_{1st} (°ATDC)	−32 to −21	−30
Δ_1 (= spark timing − SOI_{1st}) (°ATDC)	0 to 3	1
SOI_{2nd} (°ATDC)	−25 to −4	−16

3.2. Effect of Injector Clocking

First, the injector clocking angle was varied from −20 to 20°, where the negative sign denoted clockwise rotation and the positive number represented counterclockwise rotation, as shown in Figure 3. It is also worth mentioning that the swirl motion followed a clockwise direction. Note that the baseline injector clocking angle was 0°.

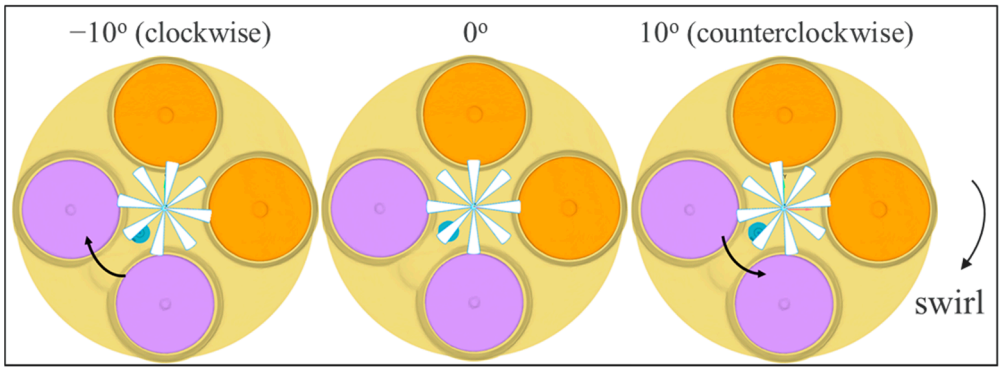

Figure 3. Layout of three different injector clocking angles (from left to right: −10, 0, and 10°).

The global combustion characteristics in terms of combustion efficiency and combustion phasing (CA2, CA10, and CA50) are shown in Figure 4. CA2 and CA10, defined as the crank angle at which 2 and 10%, respectively, of the total heat release was attained, delineated the early-stage ignition facilitated by spark assistance. Meanwhile, CA50 was defined as the crank angle when 50% of the total heat release was reached, associated with the main combustion occurred in late stage.

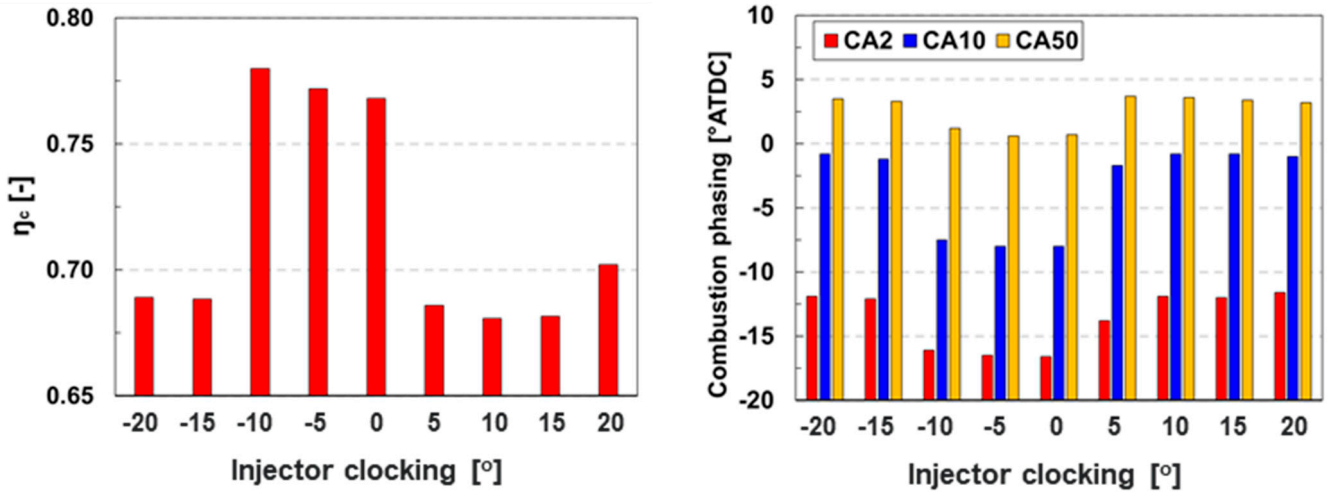

(**a**) (**b**)

Figure 4. Effect of injector clocking on (**a**) combustion efficiency (η_c) and (**b**) combustion phasing (CA2, CA10, and CA50).

It can be seen that the best combustion efficiency was shown at an injector clocking angle between −10 and 0°. Combustion phasing (CA2 to CA50) was also most advanced within this clocking angle range. Previous work [22] demonstrated that the interaction between the spark plug electrode and spray plume significantly affected the flame kernel development and the local fuel–air mixing process, thus influencing the entire subsequent combustion process. At the current spark plug location, there was no physical interaction between spray plume and spark plug surface when the injector clocking angle was smaller than −10 or larger than 10°.

To further examine the effect of the injector clocking angle on ignition, the flame kernel development, the equivalence ratio (Φ), and velocity flow fields at an injector clocking angle range of −10 to 10° were characterized (Figure 5). It was clearly evident that the spray plume and the spark plug interacted differently. The shape of the flame kernel and the size of the flame region were also different. At the −10° injector clocking angle, the flame kernel grew outside of the spark gap and was guided toward a locally richer fuel–air mixture region following the swirl motion. The flame region then continued to expand. Conversely, at the 10° injector clocking angle, the flame kernel initially formed and developed near the spark gap. However, as the flame kernel expanded outside of the spark gap, it moved into a locally leaner mixture region. The size of the flame region then became smaller and eventually quenched.

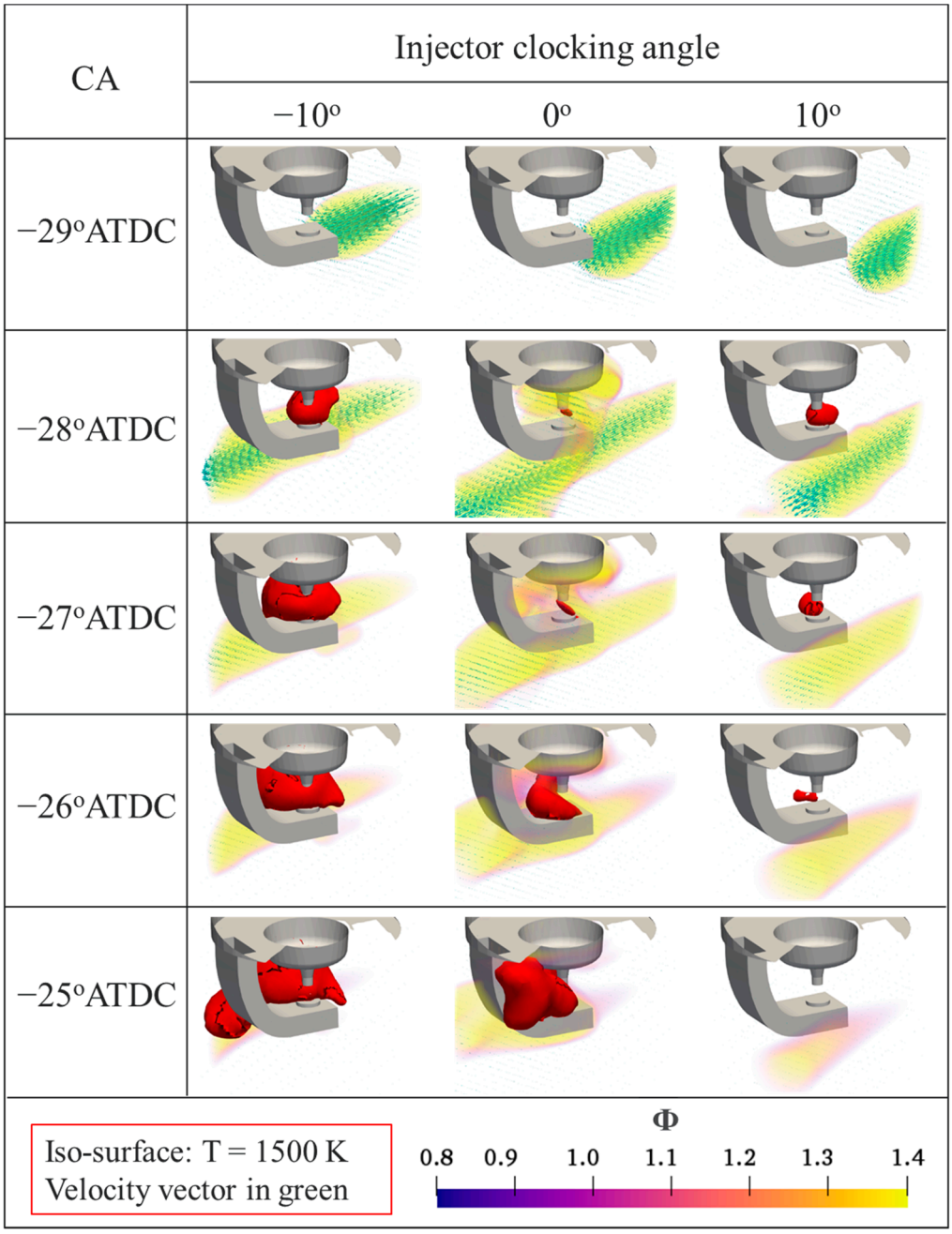

Figure 5. Flame kernel development, equivalence ratio (Φ) distribution, and velocity flow field of three different injector clocking angles (−10, 0, and 10°) at different crank angles (−29 to −25° ATDC).

In a previous study [22], an ignitable mixture volume, formulated on the cylinder charge volume of a temperature ranging from 1000 to 1500 K and a Φ ranging from 0.8 to 1.4, was introduced to characterize the early flame development and signify the mixture that was favorable for ignition. Figure 6 shows the ignitable mixture volume at different injector clocking cases at 5°CA after spark timing. Aligned with observations in Figure 5, the −10° clocking angle clearly had the largest ignitable mixture volume because of the sustainable flame kernel, while a lower ignitable mixture volume was shown in the 5 and 10° cases due to the suppressed flame kernel. This resulted in the unfavorable early ignition near spark gap and late main combustion in the 5 and 10° injector clocking cases, in turn producing the lower combustion efficiencies.

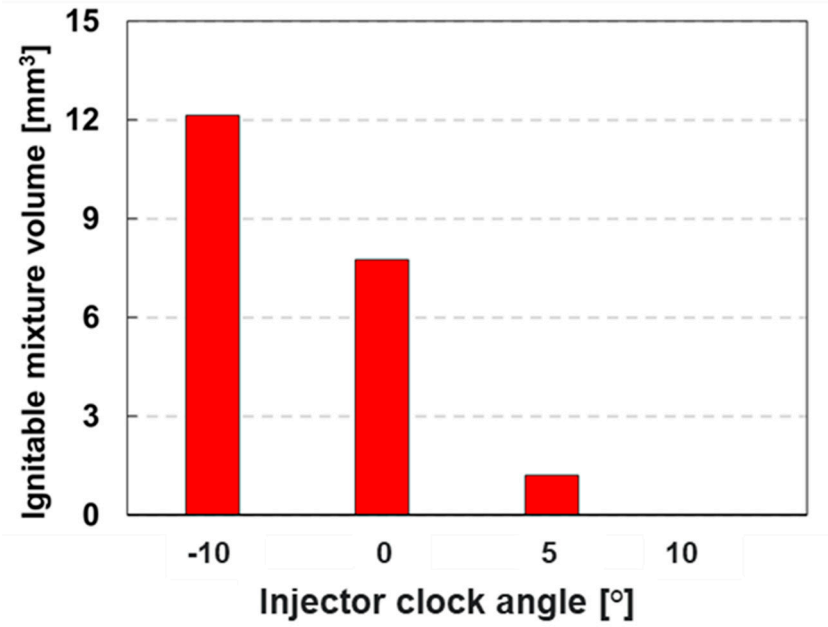

Figure 6. Effect of injector clocking on ignitable mixture volume at 5°CA after spark timing.

3.3. Effect of Number of Nozzle Holes

The effect of the number of nozzle holes on flame kernel growth and combustion performance was evaluated by varying it from 7 to 12 holes. Figure 7 displays a sample layout of 8- and 12-hole nozzles. For the different number of nozzle holes, the total nozzle area and total injected mass remained the same. Therefore, as the number of nozzle holes increased, the nozzle diameter decreased and the injected mass from each nozzle hole also decreased. Note that the baseline number of nozzle holes was 8.

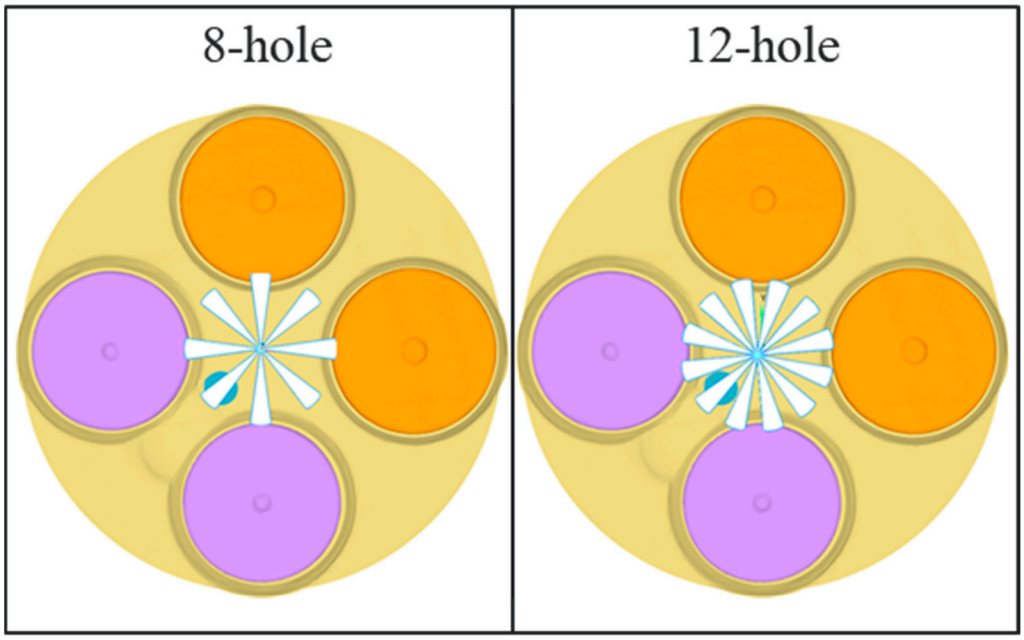

Figure 7. Layout of two different nozzles (8- and 12-hole).

Figure 8 shows the effect of the number of nozzle holes on combustion efficiency and combustion phasing (CA2, CA10, and CA50). In general, combustion efficiency increased and combustion phasing advanced with the increase in number of nozzle holes. The 12-hole case showed the highest combustion efficiency and the most advanced combustion.

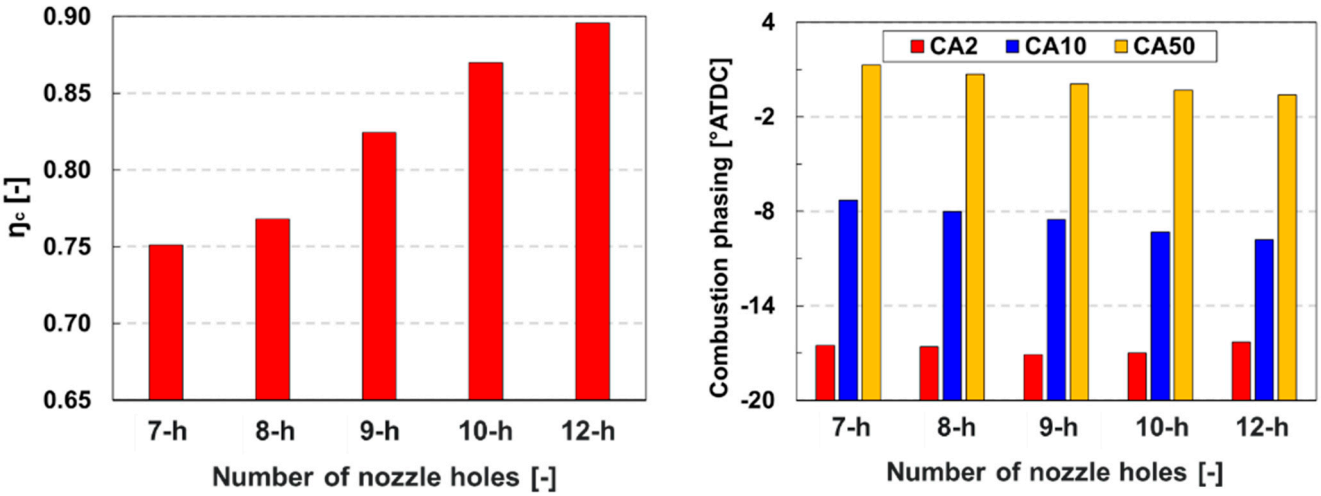

(**a**) (**b**)

Figure 8. Effect of number of nozzle holes on (**a**) combustion efficiency (η_c) and (**b**) combustion phasing (CA2, CA10, and CA50).

Figure 9 shows the effect of the number of nozzle holes on flame kernel development and equivalence ratio and velocity flow fields. As the number of nozzle holes increased from 8 to 12, the flame kernel was generated and grew continuously to a direction slightly apart from the spark gap. The size of flame volume was different due to the fuel injection quantity per plume and the resulting difference in fuel–air mixture formation. In addition to the smaller nozzle diameter and less injected mass in the 12-hole case, the effect of swirl motion on local flow field was also stronger in the 12-hole case, leading to a better spray evaporation and fuel–air mixing process. The temporal ignitable mixture volume in Figure 10 also supports this argument. It was clear that the early combustion indicated by a higher ignitable mixture volume showed at the 12-hole case led to the earlier ignition than the other cases.

3.4. Effect of Spray Inclusion Angle

The impact of spray inclusion angle on flame kernel development and combustion process was evaluated by varying the angle from 140 to 156°. Note that the baseline spray inclusion angle was 148°. As seen in Figure 11, 148° produced the highest combustion efficiency and the most advanced combustion phasing.

Figure 12 shows the flame kernel development, equivalence ratio distribution, and velocity flow field at various spray inclusion angles. When increasing the spray inclusion angle from 144 to 148°, the size of the flame region continuously grew near the spark gap region due to the spark-assisted early combustion. Correspondingly, combustion efficiency was enhanced and combustion phasing was advanced. Although the physical interaction between the spray plume and the spark plug was present, increasing the spray inclusion angle beyond 150° resulted in a large portion of the fuel spray being directed right into the spark gap area (especially at 156°), leading to flame kernel suppression and quenching. As a result, combustion efficiency was lowered along with retarded combustion phasing.

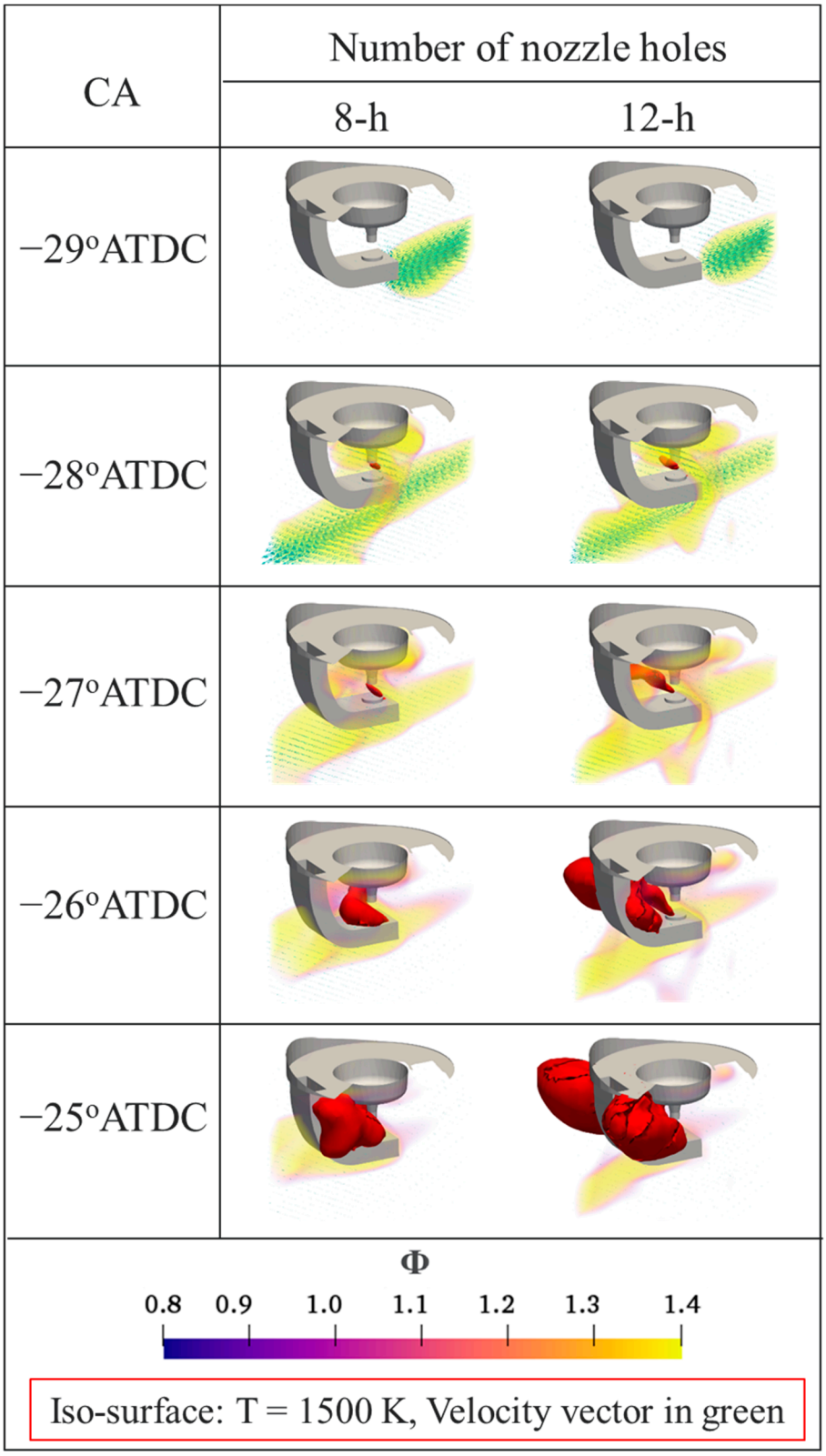

Figure 9. Flame kernel development, equivalence ratio (Φ) distribution, and velocity flow field of different numbers of nozzle holes (8- and 12-hole) at different crank angles (−29 to −25°ATDC).

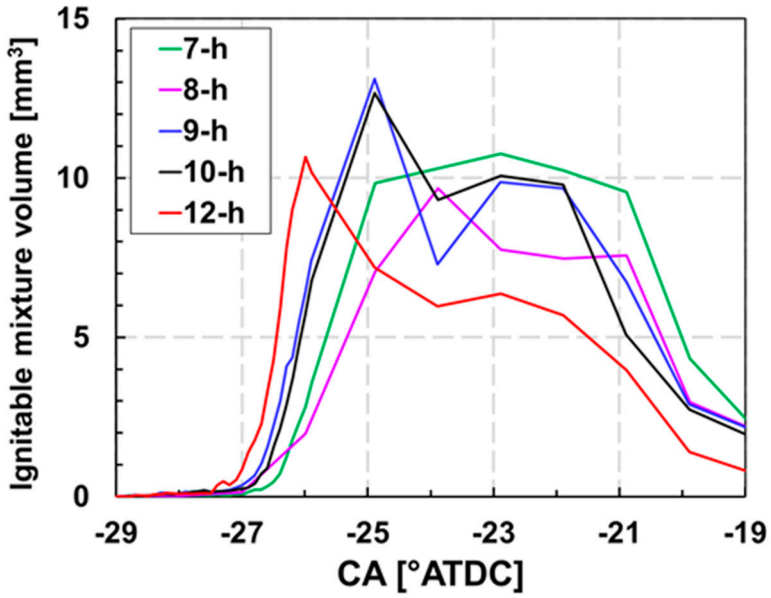

Figure 10. Effect of number of nozzle holes on ignitable mixture volume.

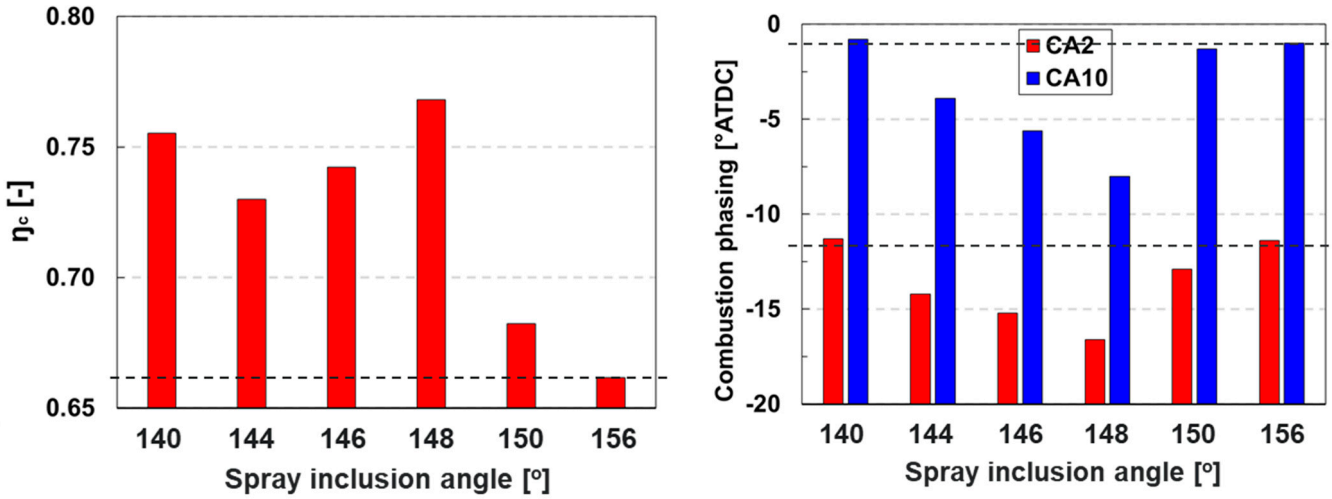

(**a**) (**b**)

Figure 11. Effect of spray inclusion angle on (**a**) combustion efficiency (η_c) and (**b**) combustion phasing (CA2 and CA10).

Figure 13 shows the effect of spray inclusion angle on the ignitable mixture volume at early ignition stage. When the spray inclusion angle was below 148°, the flame volume sustained for a short time but dropped down to zero afterward. The ignitable mixture volume in the 148° case was higher than those for other cases. This was consistent with the findings described in Figure 12. Early combustion hardly happened in the 150 and 156° cases and the ignitable mixture volume was almost zero.

3.5. Effect of Fuel Split Ratio

The effect of fuel split ratio on flame development and mixture distribution near the spark plug was also investigated. Both single and split injection strategies were studied. The split ratio was varied from 2:8 to 7:3. As the split ratio varied, the injected mass and injection duration at both pilot and main injection events also varied. To ensure the fairness of ignition and combustion progressions in each case, we also varied spark timing according to the time difference between the pilot injection duration of the target case and

baseline case. For instance, taking the baseline split ratio of 4:6 as a reference, the spark timing was advanced when the split ratio was 3:7 but it was retarded when the split ratio was 7:3.

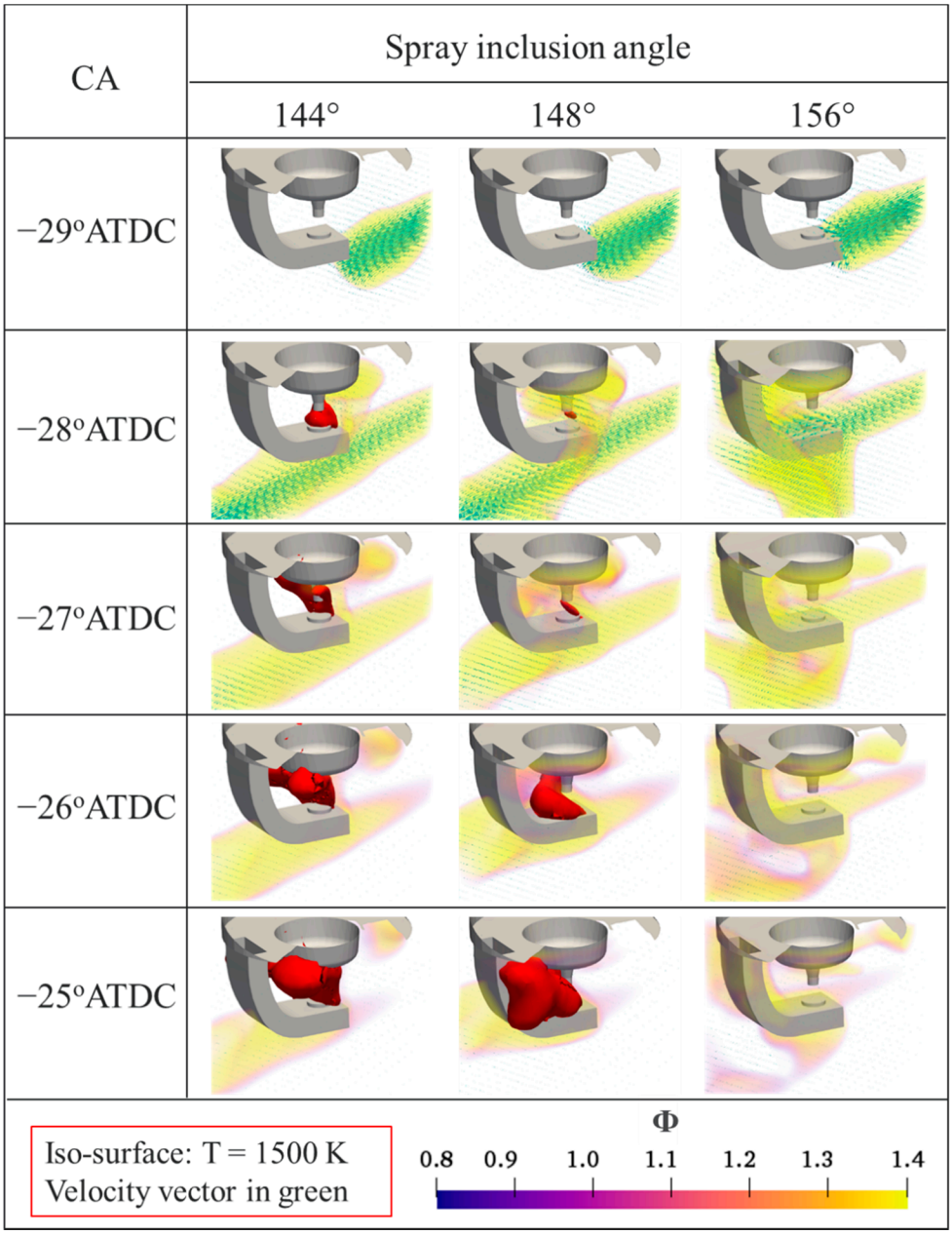

Figure 12. Flame kernel development, equivalence ratio (Φ) distribution, and velocity flow field of different spray inclusion angles (140 to 156°) at different crank angles (−29 to −25° ATDC).

Figure 14 shows that a split ratio of 2:8 led to the highest combustion efficiency (~87%). The 2:8 split ratio also corresponded to the most advanced CA50. In comparison, the single injection strategy had the lowest combustion efficiency and the most retarded CA50. This finding aligned with previous investigations [17,21,22], in which split injection strategies have been commonly employed at cold conditions to improve ignitibility and stability. Additionally, during cold start in either spark ignition (SI) or compression ignition (CI) engine, hydrocarbon (HC) emissions decreased with the split injection strategies as compared to single injection.

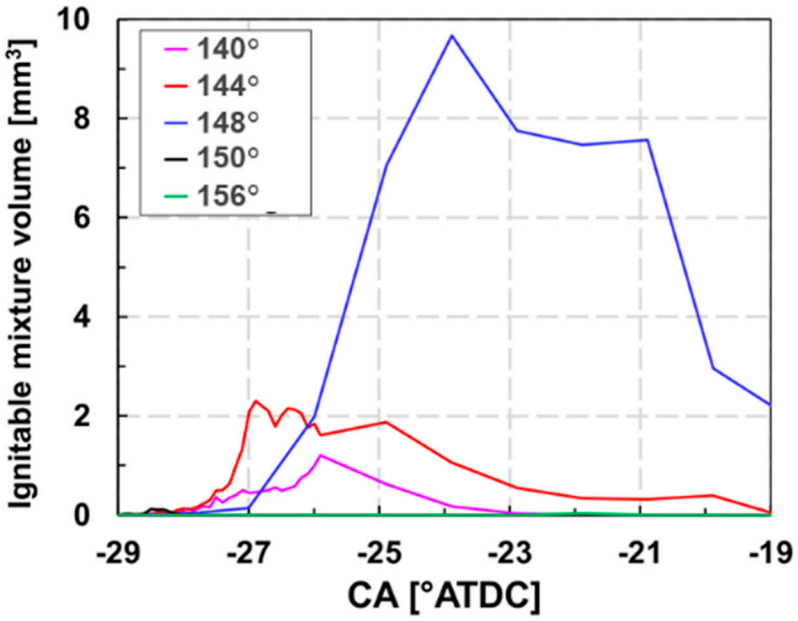

Figure 13. Effect of spray inclusion angle on ignitable mixture volume.

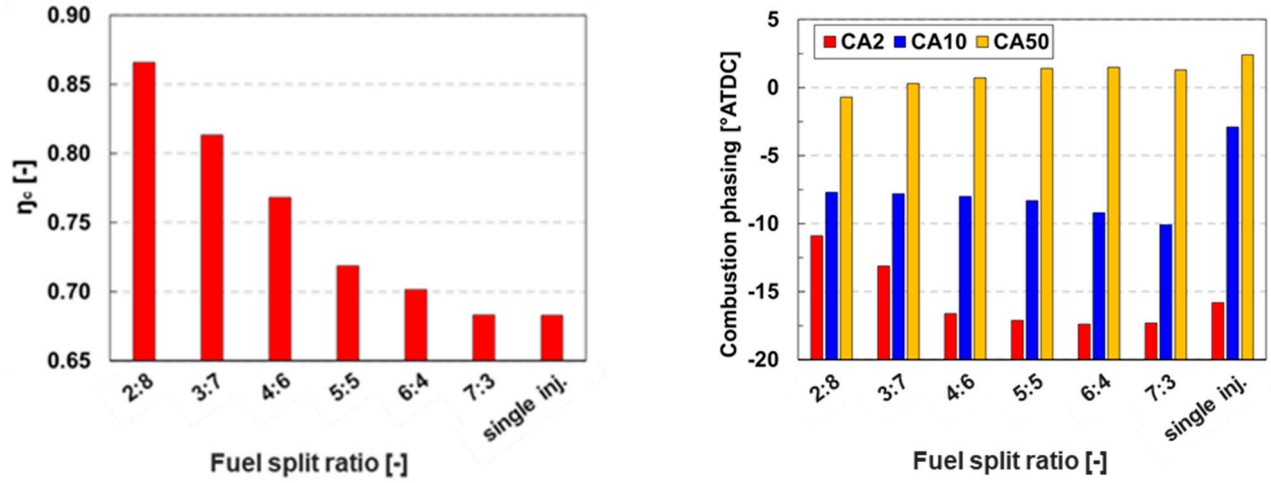

(**a**) (**b**)

Figure 14. Effect of fuel split ratio on (**a**) combustion efficiency (η_c) and (**b**) combustion phasing (CA2, CA10, and CA50).

Figure 15 shows three split ratios selected to illustrate the influence of fuel split ratio on flame kernel development and equivalence ratio distribution. It was clear that the flame kernel formation and flame propagation occurred in all three cases. Figure 16 shows that the split ratio of 2:8 had the earliest rise in ignitable mixture volume.

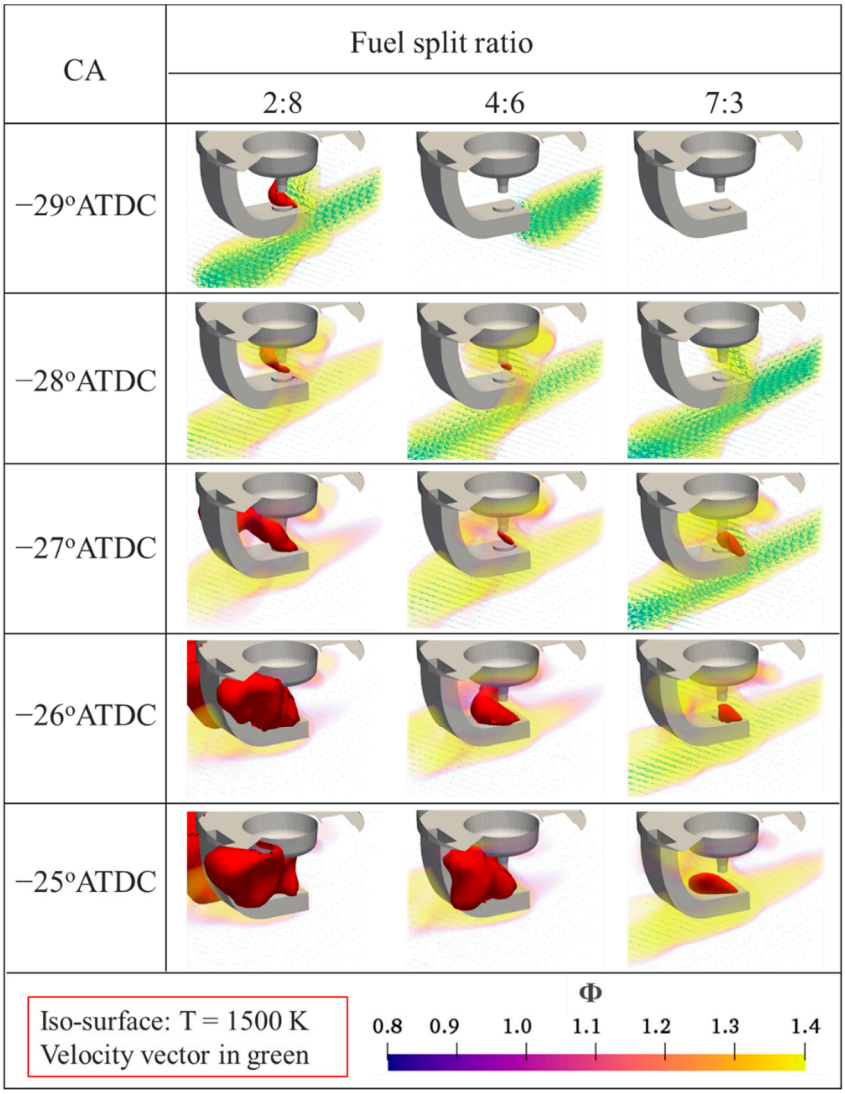

Figure 15. Flame kernel development, equivalence ratio (Φ) distribution, and velocity flow field of three different fuel split ratios (2:8, 4:6, and 7:3) at different crank angles (−29 to −25°ATDC).

3.6. Effect of Fuel Injection Strategy

As stated above, the split injection strategy performed better than the single injection strategy. Thus, it was subjected to further detailed investigation. First, the influence of the start of the first injection timing (SOI_{1st}) was examined. Spark timing is important for early flame development. Moreover, the relationship between spark timing and SOI_{1st} is critical for local fuel–air mixture formation and the subsequent combustion process [21]. Therefore, a parameter, Δ_1, that represented the difference between spark timing and SOI_{1st} was introduced. Our baseline condition was $\Delta_1 = 1$, with respect to the $SOI_{1st} = -30°$ATDC and the spark timing = −29°ATDC.

While keeping Δ_1 at 1, the SOI_{1st} was varied from −32 to −21°ATDC. Note that the reason for setting the upper boundary of SOI_{1st} to −21°ATDC was to ensure enough spare time before the second injection started. Combustion performance characteristics, including combustion efficiency and combustion phasing, are illustrated in Figure 17. The in-cylinder pressure and AHRR are shown in Figure 18. Overall, as both spark timing and SOI_{1st} were retarded, the combustion efficiency increased progressively to near 90%, and the peak in-cylinder pressure and AHRR also increased. The lower combustion efficiency and more retarded combustion phasing were attained at $SOI_{1st} = -32°$ATDC. This was because a too early injection resulted in an unfavorable local environment for fuel–air mixing.

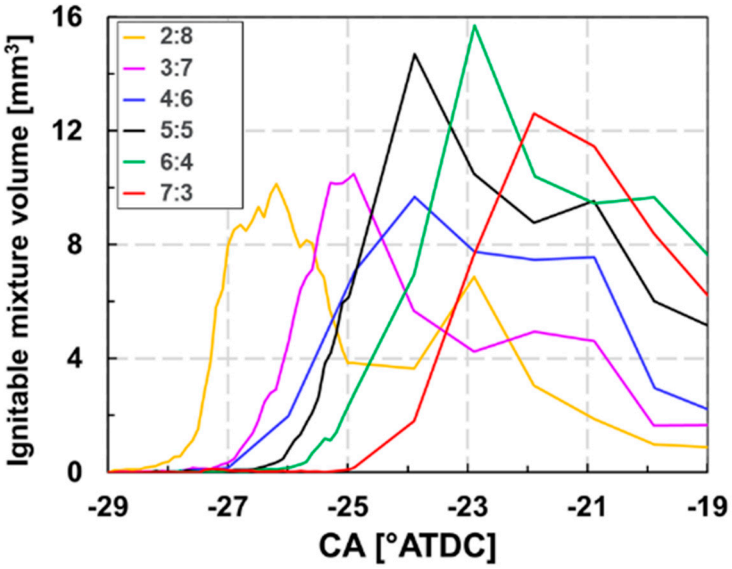

Figure 16. Effect of fuel split ratio on ignitable mixture volume.

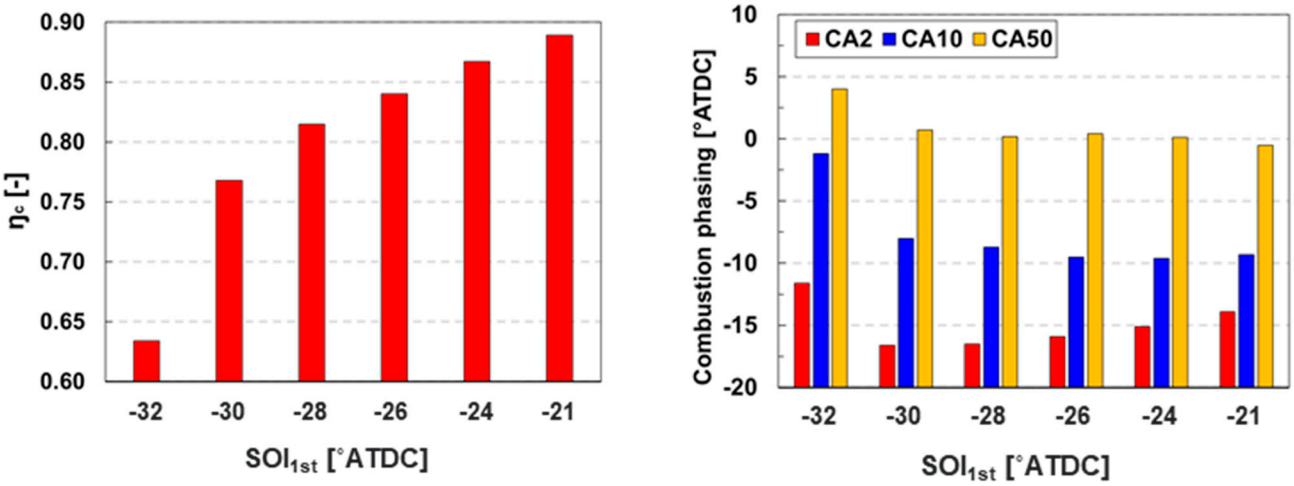

(**a**) (**b**)

Figure 17. Effect of the start of the first injection timing (SOI_{1st}) on (**a**) combustion efficiency (η_c) and (**b**) combustion phasing (CA2, CA10, and CA50) at $\Delta_1 = 1$.

To further evaluate the effect of Δ_1, it was varied from 0 to 3 at the SOI_{1st} of −30° ATDC. Figure 19 shows the effects of Δ_1 on (a) combustion efficiency and (b) combustion phasing. The highest combustion efficiency and the most advanced combustion phasing were produced at $\Delta_1 = 1$, followed by $\Delta_1 = 2$, then $\Delta_1 = 3$. When setting the sparking timing equal to SOI_{1st} (i.e., $\Delta_1 = 0$), due to the lack of localized ignition, the combustion efficiency and combustion phasing remained nearly the same as the one with no spark assistance.

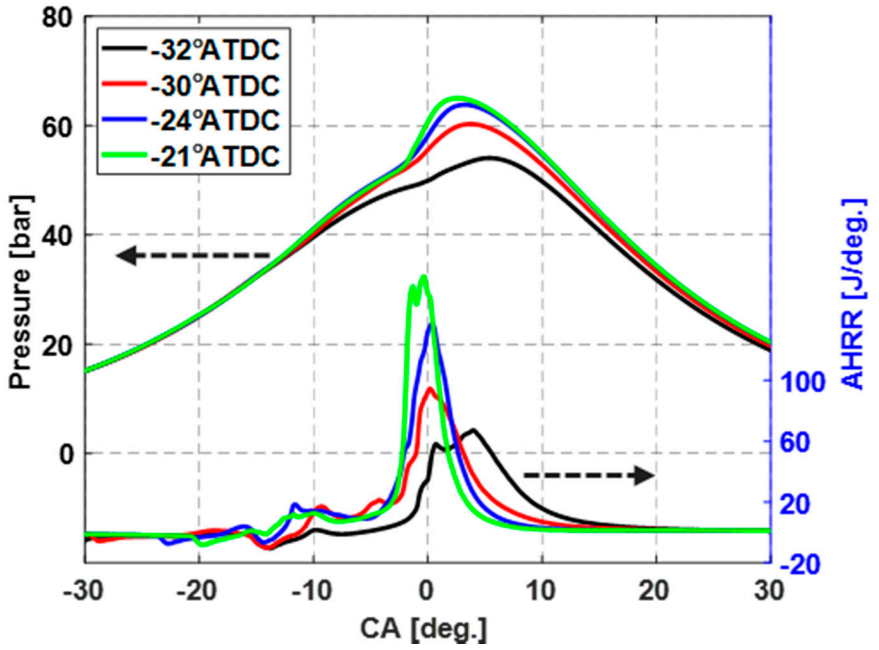

Figure 18. Effect of the start of the first injection timing (SOI_{1st}) on in-cylinder pressure and apparent heat release rate (AHRR).

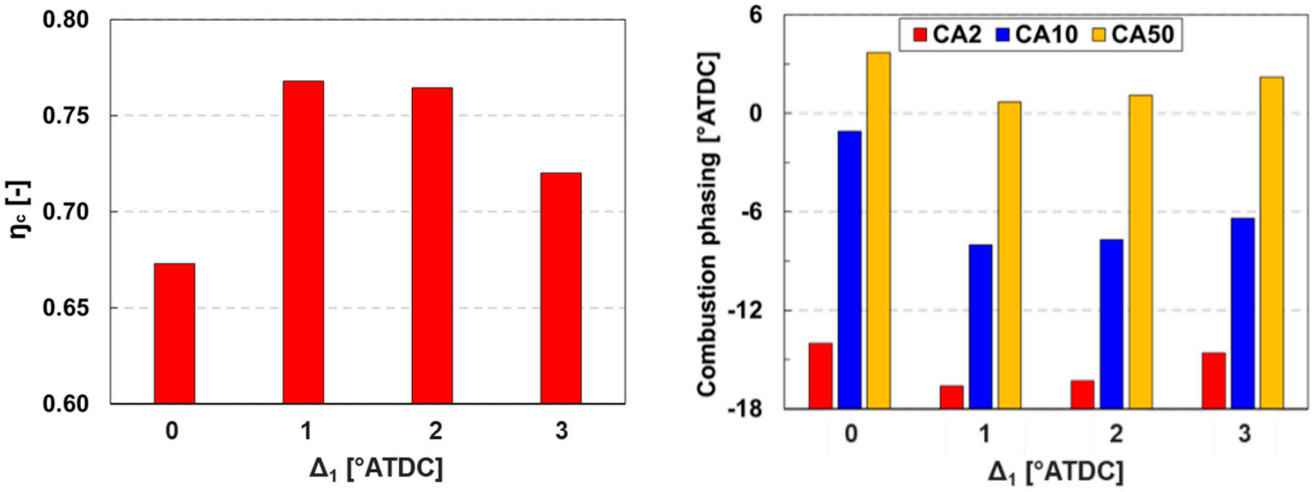

(**a**) (**b**)

Figure 19. Effect of Δ_1 on (**a**) combustion efficiency (η_c) and (**b**) combustion phasing (CA2, CA10, and CA50) at SOI_{1st} = −30° ATDC.

Thereafter, the start of the second injection timing (SOI_{2nd}) was advanced to −23° ATDC regarding the baseline condition (SOI_{2nd} = −16° ATDC), in order to evaluate its effect on the spark-assisted early ignition. Note that the spark timing and SOI_{1st} remained the same as the baseline condition (SOI_{1st} = −30° ATDC; spark timing = −29° ATDC). Figure 20 shows the effect of SOI_{2nd} on (a) combustion efficiency and (b) combustion phasing. The highest combustion efficiency occurred at the SOI_{2nd} of −23° ATDC. This was because the combustion performance benefited from both the early ignition caused by spark-assistance and compression-induced autoignition. When further retarding the SOI_{2nd}, the effect of spark assistance on early ignition was moderated and the autoignition dominated the combustion process, resulting in deterioration of combustion efficiency from 85 to 75%, along with the retarded combustion phasing. As the results presented in Figures 17 and 20

demonstrate, the SOI_{2nd} was less impactful on the combustion characteristics compared to the SOI_{1st}.

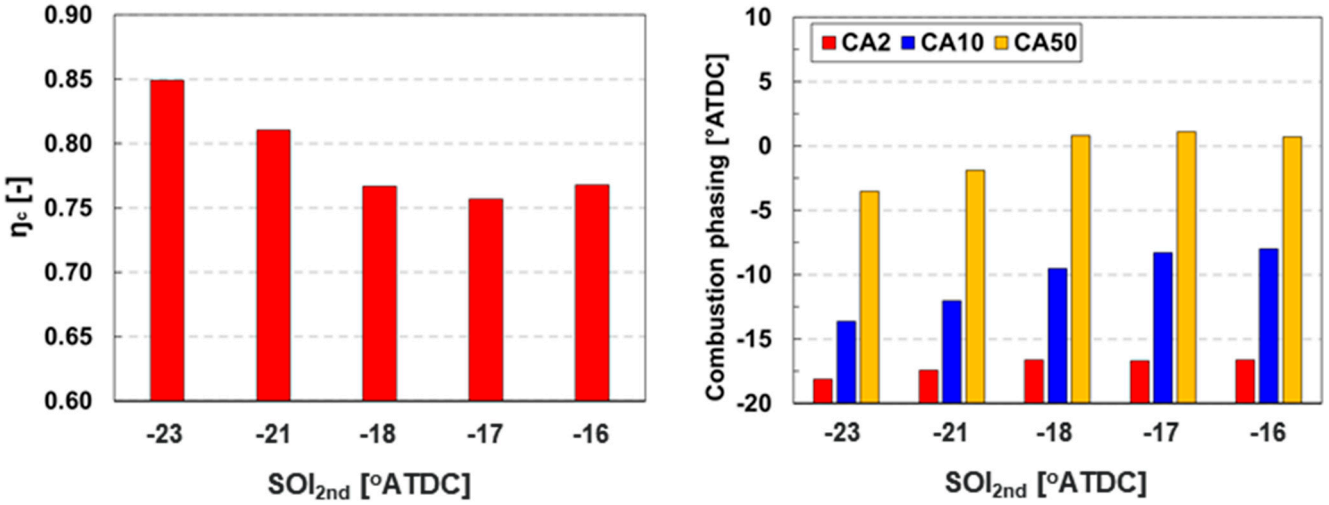

(**a**) (**b**)

Figure 20. Effect of the second start of injection timing (SOI_{2nd}) on (**a**) combustion efficiency (η_c) and (**b**) combustion phasing (CA2, CA10, and CA50).

3.7. Overview of the Spray Pattern and Fuel Injection Strategy Effects on Spark Assistance

Figure 21 provides an overview of combustion efficiency (η_c) against seven key design variables to highlight the relative importance of each design variable. The combustion efficiency values for the two baseline cases (with and without spark assistance) are highlighted in two dashed black lines.

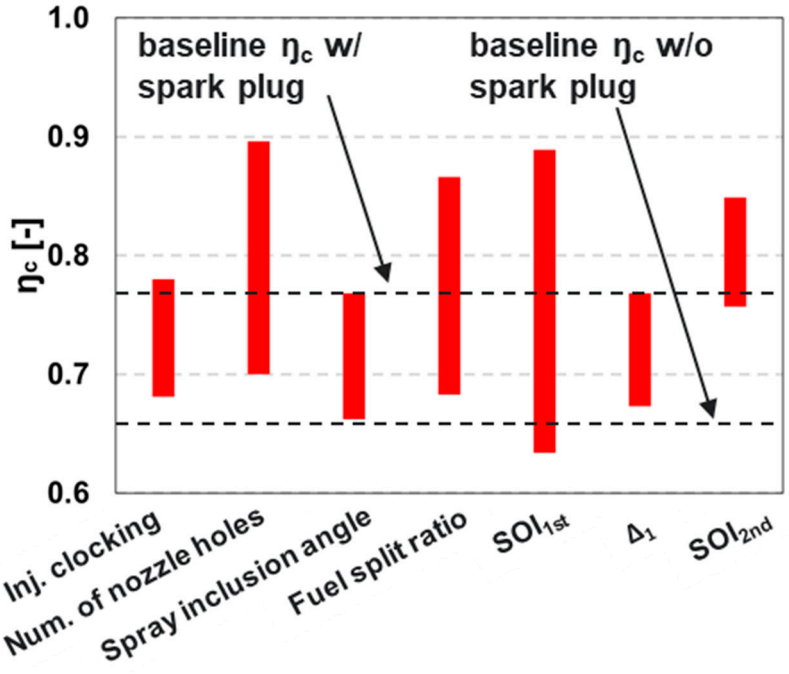

Figure 21. Combustion efficiency against seven key design variables.

Among the parameters investigated in this study, varying the number of nozzle holes could achieve the most improved combustion efficiency (~89%). With the increase in the

number of nozzle holes to 12, although the total injected mass remained the same, the nozzle diameter decreased and the injected mass from each nozzle hole was reduced. The lower spray momentum led to the most favorable fuel–air mixture formation near spark gap region, thereby facilitating flame kernel development and flame propagation.

Combustion efficiency exhibited the strongest sensitivity to the SOI_{1st}. Similar to the influence of the number of nozzle holes, the SOI_{1st} impacted both early ignition and the main combustion processes. The effect of fuel split ratio was also notable. As seen in Figure 21, injector clocking, spray inclusion angle, and Δ_1 were not as influential as other parameters on the combustion efficiency.

4. Conclusions

This study performed 3D CFD analysis to evaluate the effects of injector spray pattern and fuel injection strategy on combustion performance of a spark-assisted heavy-duty GCI engine during cold idle operations. Based on the simulation results, the major conclusions are summarized as below:

- Our analysis revealed that the spark assistance with appropriate injector spray pattern and fuel injection strategy enhanced GCI combustion at cold idle conditions. The effectiveness of spark-assisted cold starting strategy has been also reported by other researchers [32–35].
- An injector clocking angle between -10 and 0° produced the best synergy between the spray plume–spark plug interaction and swirl motion on influencing the flame kernel development and local flow field, resulting in enhanced combustion efficiency.
- Increasing the number of nozzle holes was effective in promoting combustion. Combustion efficiency increased and CA50 advanced. Twelve holes provided the best performance.
- The spray inclusion angle affected the interaction between the spark plug and spray plumes and further influenced the combustion process. A spray inclusion angle of 148° was found to be most favorable.
- The fuel split ratio affected the fuel–air mixing process and flame kernel growth. Split injections performed better than a single injection. A split ratio of 2:8 had the highest combustion efficiency.
- Combustion efficiency was notably sensitive to the SOI_{1st}. The difference between the spark timing and SOI_{1st} (i.e., Δ_1) of 1 showed the best combustion performance.
- The number of nozzle holes and fuel injection timing (SOI_{1st}) had the most significant effects on the engine combustion performance.

Author Contributions: Conceptualization, Y.Z., Y.P. and A.Z.; methodology, Y.Z., Y.P. and A.Z.; validation, L.Z.; formal analysis, L.Z.; investigation, L.Z. and M.M.A.; data curation, L.Z.; writing—original draft preparation, L.Z.; writing—review and editing, Y.Z., Y.P. and M.M.A.; supervision, Y.Z., Y.P. and M.M.A.; project administration, Y.Z. and Y.P. All authors have read and agreed to the published version of the manuscript.

Funding: This research was financially supported by Aramco Americas: Aramco Research Center-Detroit.

Institutional Review Board Statement: Not applicable.

Informed Consent Statement: Not applicable.

Data Availability Statement: Not applicable.

Conflicts of Interest: The authors declare no conflict of interest.

Nomenclature

η_c	Combustion efficiency
Φ	Equivalence ratio
φ	Spray inclusion angle
SOI_{1st}	The first start of injection
SOI_{2nd}	The second start of injection
φ	Spray inclusion angle
Δ_1	Difference between spark timing and SOI_{1st}

References

1. Andrae, J.; Brinck, T.; Kalghatgi, G. HCCI experiments with toluene reference fuels modeled by a semidetailed chemical kinetic model. *Combust. Flame* **2008**, *155*, 696–712. [CrossRef]
2. An, Y.; Jaasim, M.; Raman, V.; Pérez, F.E.H.; Sim, J.; Chang, J.; Im, H.G.; Johansson, B. Homogeneous charge compression ignition (HCCI) and partially premixed combustion (PPC) in compression ignition engine with low octane gasoline. *Energy* **2018**, *158*, 181–191. [CrossRef]
3. Epping, K.; Aceves, S.; Bechtold, R.; Dec, J.E. *The Potential of HCCI Combustion for High Efficiency and Low Emissions*; SAE Technical Paper 2002-01-1923; SAE International: San Diego, CA, USA, 2002. [CrossRef]
4. Noehre, C.; Andersson, M.; Johansson, B.; Hultqvist, A. Characterization of Partially Premixed Combustion. In Proceedings of the Powertrain & Fluid Systems Conference and Exhibition, Toronto, OB, Canada, 16–19 October 2006. [CrossRef]
5. Cho, K.; Han, M.; Wagner, R.; Sluder, C.S. Mixed-Source EGR for Enabling High Efficiency Clean Combustion Modes in a Light-Duty Diesel Engine. *SAE Int. J. Engines* **2008**, *1*, 457–465. [CrossRef]
6. Kokjohn, S.L.; Hanson, R.; Splitter, D.; Kaddatz, J.; Reitz, R.D. Fuel Reactivity Controlled Compression Ignition (RCCI) Combustion in Light- and Heavy-Duty Engines. *SAE Int. J. Engines* **2011**, *4*, 360–374. [CrossRef]
7. Prikhodko, V.Y.; Curran, S.J.; Barone, T.L.; Lewis, S.A.; Storey, J.M.; Cho, K.; Wagner, R.M.; Parks, J.E. Emission Characteristics of a Diesel Engine Operating with In-Cylinder Gasoline and Diesel Fuel Blending. *SAE Int. J. Fuels Lubr.* **2010**, *3*, 946–955. [CrossRef]
8. Roberts, J.; Kokjohn, S.; Hou, D.; Huang, Y. *Performance of Gasoline Compression Ignition (GCI) with On-Demand Reactivity Enhancement over Simulated Drive Cycles*; SAE Technical Paper 2018-01-0255; SAE International: Detroit, MI, USA, 2018. [CrossRef]
9. Reitz, R.D.; Duraisamy, G. Review of high efficiency and clean reactivity controlled compression ignition (RCCI) combustion in internal combustion engines. *Prog. Energy Combust. Sci.* **2015**, *46*, 12–71. [CrossRef]
10. Kalghatgi, G.T.; Risberg, P.; Angstrom, H.-E. *Partially Pre-Mixed Auto-Ignition of Gasoline to Attain Low Smoke and Low NO_x at High Load in a Compression Ignition Engine and Comparison with a Diesel Fuel*; SAE Technical Paper 2007-01-0006; SAE International: Cape Town, South Africa, 2007. [CrossRef]
11. Weall, A.; Collings, N. *Investigation into Partially Premixed Combustion in a Light-Duty Multi-Cylinder Diesel Engine Fuelled with a Mixture of Gasoline and Diesel*; SAE Technical Paper 2007-01-4058; SAE International: Rosemont, IL, USA, 2007. [CrossRef]
12. Sellnau, M.; Sinnamon, J.; Hoyer, K.; Husted, H. Gasoline Direct Injection Compression Ignition (GDCI)—Diesel-like Efficiency with Low CO_2 Emissions. *SAE Int. J. Engines* **2011**, *4*, 2010–2022. [CrossRef]
13. Cho, K.; Latimer, E.; Lorey, M.; Cleary, D.J.; Sellnau, M. Gasoline Fuels Assessment for Delphi's Second Generation Gasoline Direct-Injection Compression Ignition (GDCI) Multi-Cylinder Engine. *SAE Int. J. Engines* **2017**, *10*, 1430–1442. [CrossRef]
14. Dec, J.E.; Dernotte, J.; Ji, C. Increasing the Load Range, Load-to-Boost Ratio, and Efficiency of Low-Temperature Gasoline Combustion (LTGC) Engines. *SAE Int. J. Engines* **2017**, *10*, 1256–1274. [CrossRef]
15. Cho, K.; Zhao, L.; Ameen, M.; Zhang, Y.; Pei, Y.; Moore, W.; Sellnau, M. Understanding Fuel Stratification Effects on Partially Premixed Compression Ignition (PPCI) Combustion and Emissions Behaviors. In Proceedings of the WCX SAE World Congress Experience, Detroit, MI, USA, 9–11 April 2019. [CrossRef]
16. Rose, K.; Ariztegui, J.; Cracknell, R.; Dubois, T.; Hamje, H.; Pellegrini, L.; Rickeard, D.; Heuser, B.; Schnorbus, T.; Kolbeck, A. *Exploring a Gasoline Compression Ignition (GCI) Engine Concept*; SAE Technical Paper 2013-01-0911; SAE International: Detroit, MI, USA, 2013. [CrossRef]
17. Zhao, L.; Ameen, M.; Pei, Y.; Zhang, Y.; Kumar, P.; Tzanetakis, T.; Traver, M. *Numerical Evaluation of Gasoline Compression Ignition at Cold Conditions in a Heavy-Duty Diesel Engine*; SAE Technical Paper 2020-01-0778; SAE International: Detroit, MI, USA, 2020. [CrossRef]
18. Zhao, L.; Ameen, M.M.; Pei, Y.; Zhang, Y.; Traver, M.; Garcia-Oliver, J.; Vera-Tudela, W. Effect of Fuel Properties on Spray and Combustion Characteristics under Compression Ignition Engine Conditions. In Proceedings of the 11th US National Combustion Meeting, Pasadena, CA, USA, 24–27 March 2019.
19. Zhang, Y.; Kumar, P.; Pei, Y.; Traver, M.; Cleary, D. *An Experimental and Computational Investigation of Gasoline Compression Ignition Using Conventional and Higher Reactivity Gasolines in a Multi-Cylinder Heavy-Duty Diesel Engine*; SAE Technical Paper 2018-01-0226; SAE International: Detroit, MI, USA, 2018. [CrossRef]
20. Kern, C.; Dressler, W.; Lindemann, G.; Rothacker, V. *An Innovative Glow System for Modern Diesel Engines*; SAE Technical Paper 1999-01-1240; SAE International: Detroit, MI, USA, 1999. [CrossRef]

21. Zhao, L.; Pei, Y.; Zhang, Y.; Kumar, P.; Tzanetakis, T.; Traver, M.; Ameen, M. Numerical Evaluation of Spray-Guided Glow Plug Assistance on Gasoline Compression Ignition During Cold Idle Operation in a Heavy-Duty Diesel Engine. In Proceedings of the ASME Internal Combustion Engine Division Fall Technical Conference, Denver, CO, USA, 1–4 November 2020. [CrossRef]
22. Zhao, L.; Zhang, Y.; Pei, Y.; Zhang, A.; Traver, M.; Ameen, M. *Numerical Evaluation of Spark Assisted Cold Idle Operation in a Heavy-Duty Gasoline Compression Ignition Engine*; SAE Technical Paper 2021-01-0410; SAE International: Detroit, MI, USA, 2021. [CrossRef]
23. Richards, K.J.; Senecal, P.K.; Pomraning, E. *Converge Manual (Version 2.4)*; Convergent Science Inc.: Madison, WI, USA, 2018.
24. Liu, Y.-D.; Jia, M.; Xie, M.-Z.; Pang, B. Enhancement on a Skeletal Kinetic Model for Primary Reference Fuel Oxidation by Using a Semidecoupling Methodology. *Energy Fuels* **2012**, *26*, 7069–7083. [CrossRef]
25. Zhang, Y.; Pei, Y.; Tang, M.; Traver, M. A Computational Investigation of Piston Bowl Geometry and Injector Spray Pattern Effects on Gasoline Compression Ignition in a Heavy-Duty Diesel Engine. In Proceedings of the ASME Internal Combustion Engine Division Fall Technical Conference, Chicago, IL, USA, 20–23 October 2019. [CrossRef]
26. Golovitchev, V.I.; Nordin, N.; Jarnicki, R.; Chomiak, J. *3-D Diesel Spray Simulations Using a New Detailed Chemistry Turbulent Combustion Model*; SAE Technical Paper 2000-01-1891; SAE International: Paris, France, 2000. [CrossRef]
27. Yang, J.; Golovitchev, V.; Redon, P.; Javier Lopez Sanchez, J. *Numerical Analysis of NO_x Formation Trends in Biodiesel Combustion using Dynamic ϕ-T Parametric Maps*; SAE Technical Paper 2011-01-1929; SAE International: Kyoto, Japan, 2011. [CrossRef]
28. Pei, Y.; Som, S.; Pomraning, E.; Senecal, P.K.; Skeen, S.A.; Manin, J.; Pickett, L.M. Large eddy simulation of a reacting spray flame with multiple realizations under compression ignition engine conditions. *Combust. Flame* **2015**, *162*, 4442–4455. [CrossRef]
29. Zhao, L. An Experimental and Computational Study of Fuel Spray Interaction: Fundamentals and Engine Applications. Ph.D. Thesis, Michigan Technological University, Houghton, MI, USA, 2018.
30. Zhao, L.; Moiz, A.A.; Som, S.; Fogla, N.; Bybee, M.; Wahiduzzaman, S.; Mirzaeian, M.; Millo, F.; Kodavasal, J. Examining the role of flame topologies and in-cylinder flow fields on cyclic variability in spark-ignited engines using large-eddy simulation. *Int. J. Engine Res.* **2017**, *19*, 886–904. [CrossRef]
31. Som, S.; D'Errico, G.; Longman, D.E.; Lucchini, T. *Comparison and Standardization of Numerical Approaches for the Prediction of Non-reacting and Reacting Diesel Sprays*; SAE Technical Paper 2012-01-1263; SAE International: Detroit, MI, USA, 2012. [CrossRef]
32. Cracknell, R.; Bastaert, D.; Houille, S.; Châtelain, J.; Larguier, O.; Beaugé, Y.; Gente, F.; Nicolas, B.; Prevet, S.; Fandakov, A.; et al. *Assessing the Efficiency of a New Gasoline Compression Ignition (GCI) Concept*; SAE Technical Paper 2020-01-2068; SAE International: Krakow, Poland, 2020. [CrossRef]
33. La Rocca, A.; Macmillan, D.; Shayler, P.; Murphy, M.; Pegg, I. *CFD Investigation on the Influence of In-Cylinder Mixture Distribution from Multiple Pilot Injections on Cold Idle Behaviour of a Light Duty Diesel Engine*; SAE Technical Paper 2014-01-2708; SAE International: Birmingham, UK, 2014. [CrossRef]
34. Reuss, D.L.; Kuo, T.-W.; Silvas, G.; Natarajan, V.; Sick, V. Experimental metrics for identifying origins of combustion variability during spark-assisted compression ignition. *Int. J. Engine Res.* **2008**, *9*, 409–434. [CrossRef]
35. Naganuma, K.; Tanaka, K.; Ito, T.; Kobashi, Y. *Study for Ignition Characteristics and Potential of Gasoline Autoignition Combustion with Spark Assist*; SAE Technical Paper 2019-01-2317; SAE International: Kyoto, Japan, 2019. [CrossRef]